

MEASUREMENT OF HIGHER MULTIPOLE COMPONENTS IN QUADRUPOLE MAGNET

A. Ando, K. Hosono, M. Kibayashi, and M. Tsukihara*

Research Center for Nuclear Physics, Osaka University, Ibaraki, Osaka 567

*Sumitomo Heavy Industries, Ltd.,

Accelerator Business Center, Technical Department,

Niihama, Ehime 792

Abstract

Higher multipole components of a quadrupole magnet were directly measured by the fast Fourier transformation of the signal from a rotating coil, and compared with the results of polynomial fitting for the field mapping data in the medium plane by a Hall generator.

Quadrupole magnet

The full scale model of the quadrupole magnet was designed and constructed for the design study of the multipurpose storage ring (MSR) in RCNP¹. The parameters of this model are given in Table 1. The core material is the silicon steel S-23 of the Japanese Industrial Standard. Each core was stamped out from the 0.5 mm thick sheet. Also the 0.35 mm thick sheet was used to adjust the stucked core length. The pole face contour is similar to that of the main quadrupole magnet of the KEK 12-GeV proton synchrotron², except that our magnet has the symmetry between the horizontal direction and the vertical one.

Table 1. Parameters of quadrupole magnet

Maximum field	2.0	T/m
Core length (L_C)	0.4	m
Bore radius (r_B)	50	mm
Maximum current	770	A
Resistance	35	m Ω
Inductance	33	μ H _{ry}

Field measuring system

The block diagram of the field measuring system is shown in Fig.1. The pickup coil is rotated at 30 Hz by the AC 100 V synchronous motor. The signal from the coil is sampled and converted to the digital datum at every external clock. The rod mounted at the rotating axis makes the trigger signal at every passage through the photo-interrupter. At first, the control computer, PC-9801VX, gives the digitizer the number of the data to be taken, then the start command. The digitizer makes the digital datum train by A/D conversion from the first trigger signal after the start command. The analog signal between -5 V and +5 V is converted to the integer from 0 to 4095. The typical frequency of the external clock is 4096 Hz.

The short and the long rotating coil are used for the pickup. The parameters of these coils are given in Table 2.

Table 2. Parameters of rotation coil

		Short	Long
Radius (a)	mm	37.55	41.53
Length (L)	mm	10	1000
Turns (M)		12	1

Principle of measurement

The magnetic field inside the magnet is considered as two dimensional, for the uniformity along the magnet axis (z -direction). The field is described by the z -component of vector potential, A_z . Expanding A_z as

$$A_z = - \sum_{n=1}^{\infty} A_n r^n \cos(n\theta + \chi_n),$$

where the cylindrical coordinates (r, θ, z) are chosen, and A_n and χ_n are the amplitude and the phase of the $2n$ -th multipole field, we obtain the pickup signal from the rotating coil as $V = \sum_{n=1}^{\infty} V_n$ where

$$V_n = \omega M L n a^n A_n \sin(n\theta + \chi_n).$$

Here $\theta = \omega t$, ω is the angular frequency of the rotation, and a , M and L are the radius, turns and the length of the rotating coil, respectively.

The differential coefficient of the field at the magnet center is then given by

$$|B^{(n-1)}| = \left| \frac{d^{(n-1)} B_y}{dx^{(n-1)}} \right| = \frac{(n-1)! V_n}{\omega M L a^n}.$$

We can easily obtain the strength of V_n by the spectral analysis of the signal V . In this method, the main term A_m , for example A_2 in a quadrupole magnet, does not disturb the higher order signals V_n ($n > m$) as far as the rotation is stable.

Data reduction

An example of the spectra obtained by the fast Fourier transformation (FFT) is shown in Fig.2. The spectra are unfortunately not the sum of the harmonics of the rotation frequency, since the total sampling time is not exactly the multiple of the rotation period. In such a case, the spectral shape is given by

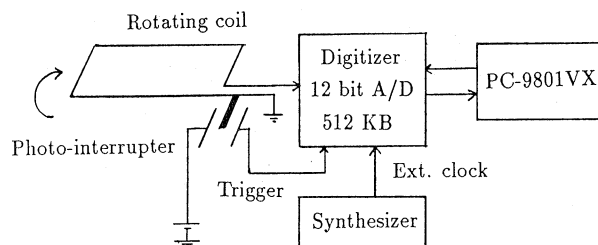


Fig. 1 Block diagram of measuring system.

$$\frac{\sin X}{X}, \quad X = \frac{\omega_n - \omega}{2} T,$$

where ω_n is the angular frequency of each spectrum, and T is the total sampling time.

In this measurement we took typically 4096 data in $T = 1 \text{ sec}$. We replaced V_2 by the $\sqrt{2}V_D$ where V_D was the read-out strength when the signal is directly input to the digital volt meter. For farther analysis, we are preparing a fitting program to obtain the true amplitude from the discrete spectra.

The dipole component is explained by the setting error of the rotation coil. The r.m.s. of the distance between the magnet axis and the rotation one is estimated as 0.25 mm .

The strength of the field gradient, $G = dB_y/dx$, and the effective length, L_g , are plotted in Fig.3 and Fig.4 for some levels of the excitation current, I . G/I in Fig.3 agrees well with the calculated value, 3.116×10^{-2} , from Table 1. From Fig.4, the effective length is approximated as

$$L_g = L_C + 1.15 r_B.$$

Higher multipoles

We define the normalized strength of the higher multipole component as

$$S_n = \frac{d^{(n-1)}B_y/dx^{(n-1)}}{G} \quad (m^{-(n-2)}),$$

$$L_n = \int \frac{d^{(n-1)}B_y/dx^{(n-1)}}{G} dz / \int G dz \quad (m^{-(n-2)}).$$

We can only find S_n , $n = 2 + 4k$ as the significant components at the center of the magnet. This suggests that the magnet is almost completely symmetric inside the radius of the rotation coil (37.55 mm). The variation of S_6 due to the excitation current is shown in Fig.5.

For the integral strength, i.e., the data of the long coil, we cannot distinguish $V_n (n \geq 7)$ from the noise level. Table 3 summarizes $L_n (n \leq 6)$ for the various currents.

Table 3. Multipole components in effective length

I (A)	L_3 ($\times 10^{-2} m^{-1}$)	L_4 ($\times 10^{-1} m^{-2}$)	L_5 ($\times 10 m^{-3}$)	L_6 ($\times 10^4 m^{-4}$)
300	1.28	7.10	5.93	9.16
250	2.28	8.86	7.46	7.84
200	-	-	7.0	8.11
150	-	-	6.81	7.19
100	-	-	7.01	8.21
50	-	-	-	10.1

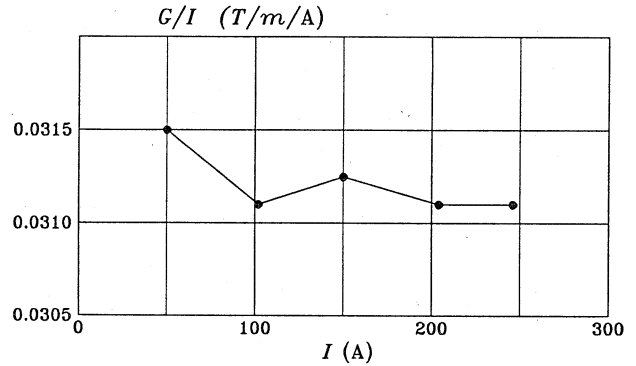


Fig. 3 Excitation curve of the field gradient.

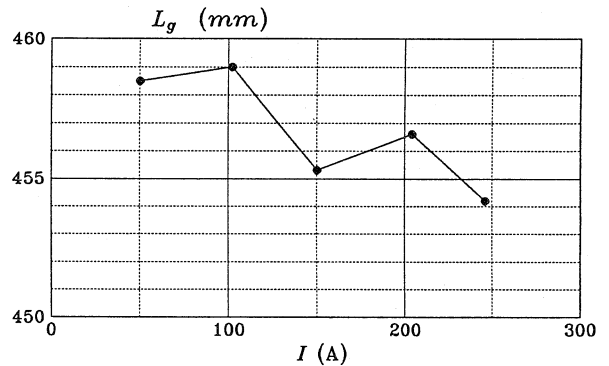


Fig. 4 Effective length versus excitation current.

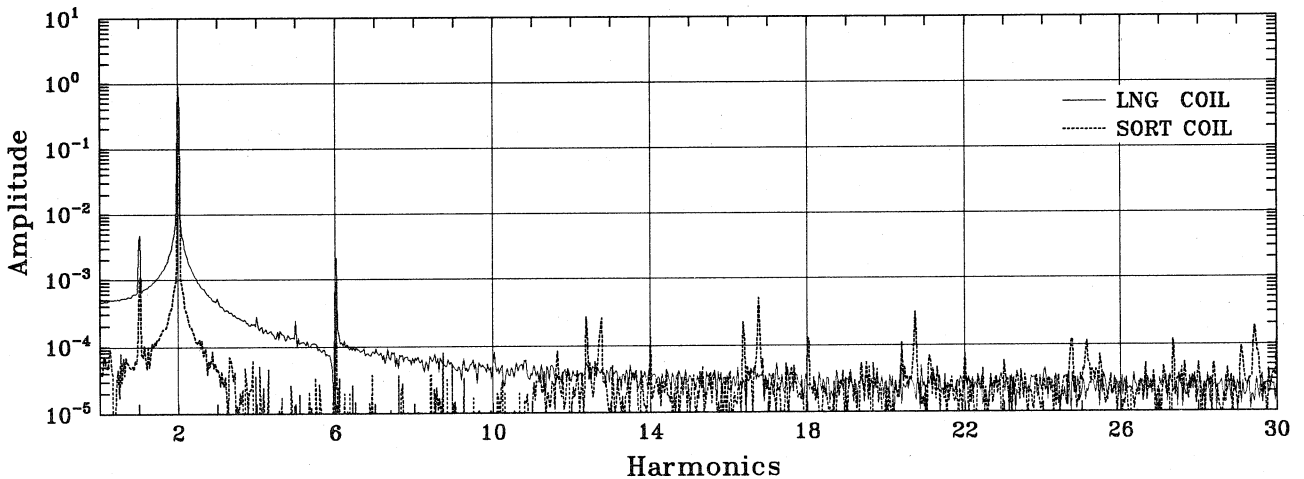


Fig. 2 Typical spectra of FFT.

From these results, the effect of the fringing field becomes important for $I > 200$ A or $G \geq 6.0$ T/m. S_n in the fringing region are measured by changing the location of the short coil from the edge of the magnet core. The results are shown in Fig.6 where "d < 0" means "inside the magnet". We measured these unfortunately at $I = 200$ A because of the cooling problems for the larger excitation current. We cannot distinguish any spectrum at $n = 3, 6, 7$ and 9 .

The 16-th multipole component ($n = 8$) seems to be mainly caused by the return flux of the fringing field. A field clamp or an end plate can completely compensate this component though this effect in L_g is negligibly small. To reduce dodecapole component ($n = 6$), cutting the pole face seems better than attaching some end plates, since this component is enhanced at $d \simeq -r_B/2$. For the decapole component ($n = 5$) at $I = 200$ A, the integral of the fringing region is estimated as about

$$2 \times 0.1(\text{mV}) \times 75(\text{mm}) = 1.5 \times 10^{-6} \text{ Volt} \cdot \text{m},$$

which corresponds to 2.1×10^2 T/m³. On the other hand, the long coil measurement gives $L_5 = 70$ m⁻³ as shown in Table 3, that is,

$$\int |B^{(4)}| dz = 70 \times 3.116 \times 10^{-2} \times 200 \times 0.4575 \simeq 2.0 \times 10^2 \text{ T/m}^3.$$

The strength of the octupole component in Table 3 would be explained by the similar calculation as above, although this component is not seen in the small coil data. Consequently we can completely reduce the higher error field ($n \neq 2 + 4k$) by a suitable "pole-face cutting".

Comparison with another measurements

We also measured the magnetic field at $I = 88$ A with a Hall generator by mapping in the medium plane, and found the multipole components by polynomial fitting. In the fitting, we used an iterative method, in which once we found some polynomials, at the next step, we added the best term to minimize the chi-square. We only show the results for the effective length in Table 4, because at the center of the magnet, higher multipoles are too small to be distinguished which term is more meaningful. Table 4 also compares with the data of the KEK 12-GeV PS³, which are obtained by a simple polynomial fitting including terms upto $n = 14$ for the field differences given by a twin coil.

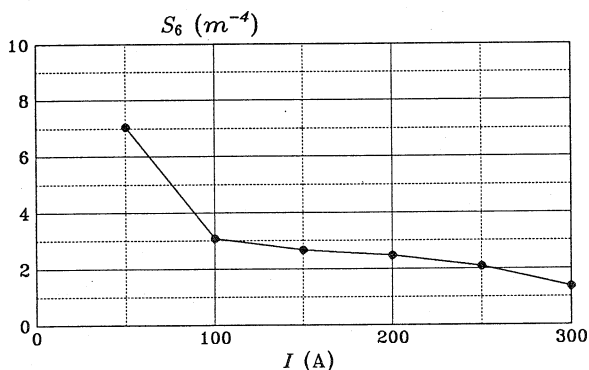


Fig. 5 Dodecapole at the magnet center versus excitation current.

Table 4. Comparison of higher multipoles in the effective length

	Rot. coil	Hall		KEK-PS
		$r \leq 50$ mm	$r \leq 80$ mm	
G (T/m)	3.12	2.74	2.74	1.28
$L_3(10^{-2}m^{-1})$	-	-3.83	-	9.2
$L_4(m^{-2})$	-	-	-1.42	0.33
$L_5(m^{-3})$	70.1	203	49.0	-70.2
$L_6(10^4m^{-4})$	8.21	-8.32	-9.88	4.89
$L_7(10^{-5}m^{-5})$	-	-	-	6.12

In the polynomial fitting, the strength of multipole components depend on the fitting procedure, that is, how many polynomial terms are included and how wide the fitting region is. The resultant coefficients couple with each other, and may lead us to misread in particular for multipoles which do not ordinary exist by the symmetry. Rotating coil method is usually available for a small region because of the magnet aperture, although higher multipoles become more important as a radius is larger. But we can correctly know multipole fields without any interference among them. The only limit is the noise-to-signal ratio. In view of beam dynamics in a synchrotron or a storage ring, the important multipoles are usually those of $n \leq 10$. As to these field, we can know their strengths (also phases) with enough accuracy by this rotating coil method.

Reference

1. A. Ando *et al.*, Proc. 6-th Symposium on Accelerator Science and Technology, 1987, p.310.
2. T. Kasuga *et al.*, Proc. Conf. on Computation of Magnetic Field, 1976, p.177.
3. A. Ando *et al.*, Proc. 9-th Int. Conf. High Energy Acc., 1974, p.610.

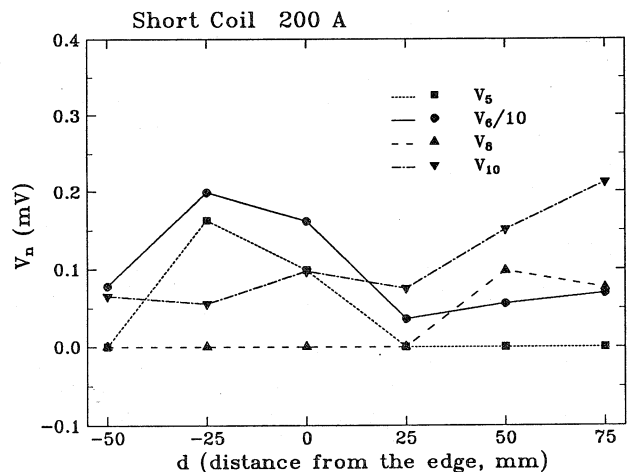


Fig. 6 Change of multipoles in the fringing region.